ICASSP 2023 - 2023 IEEE International Conference on Acoustics, Speech and Signal Processing (ICASSP) | 978-1-7281-6327-7/23/$31.00 ©2023 IEEE | DOI: 10.1109/ICASSP49357.2023.10096275

Utilization of Bessel Beams in Wideband Sub Terahertz Communication Systems to Mitigate Beamsplit Effects in the Near-field

Arjun Singh
State University of New York Polytechnic Institute
Utica, NY, USA
singha8@sunypoly.edu

Vitaly Petrov, Josep M. Jornet
Northeastern University
Boston, MA, USA
{v.petrov, j.jornet}@northeastern.edu

***Abstract*—Exploring near-field propagation is increasingly relevant for terahertz(THz)-band communications, as very large antenna arrays (VLAA) are required to overcome the large propagation losses. In the near field, the efficiency of conventional far-field beamforming is reduced, while state-of-the-art near-field beamfocusing requires perfect positioning and channel state information to work efficiently. In this paper, first, experimental measurements of wireless data transmission above 100 GHz in indoor scenarios are presented to highlight the need for VLAAs that will likely operate in the near field. Next, diffraction-free Bessel beams are described as a promising near-field contender, with propagation characteristics in the near field similar to those of beamforming in the far field. Numerical results and their interpretations highlight the impact of prospective wideband THz communications during system implementations. It is particularly observed that THz Bessel beams can be optimized for the given environment, potentially improving the performance characteristics of the system.**

***Index Terms*—6G; Beamforming; Beamfocusing; Wideband**

I. Introduction

The terahertz (THz) band (0.1 – 10 THz) has been widely researched as a promising spectral resource to augment the millimeter and microwave spectrum currently utilized in fifth-generation (5G) networks for meeting the communication needs of sixth-generation (6G) and beyond networks [1], [2]. The high photon energy and sub-millimeter wavelengths of THz signals also make them ideal for imaging and sensing.

However, THz signals suffer from extremely high path losses. On the one hand, the absorption losses, occurring at specific absorption peaks within the THz-band, act to divide the THz-band into multiple windows [3]. Nonetheless, each of these transmission windows can still provide several tens or even hundreds of GHz of contiguous bandwidth, vital for creating the ultra-broadband links that can provide support for the next generation of communication standards [4], [5]. On the other hand, the devastating spreading loss within these transmission windows severely attenuates the possible communication distance. Indeed, to make THz-band communication a viable domain, the utilization of very high gain aperture systems is vital for efficiently radiating the signal. In this scenario, the radiation is ideally concentrated in a very narrow, or so-called "pencil-like" beam [6], [7]. To ensure robust connectivity in mobile scenarios, these pencil thins beams should further be electronically steerable. Here, the utilization of very high gain arrays equipped with phase shifters could help enable the steering of these highly directional beams for securing broadband THz-communications, even in challenging mobile setups, up to several tens of meters [6].

However, the design of such systems, and their operation, become extremely challenging when trying to facilitate ultra-broadband, high-gain communications. First, the very large aperture tremendously increases the near-field region of the array, rendering canonical far-field based beamforming and beamsteering solutions ineffective, and thus calling for possible alternative near-field specific wavefronts [7]–[9]. Further, the phase shifters utilized in such implementations are, by design, narrow-band [10]–[12]. Although true-time delay lines can be explored as a possible solution to this problem [13], their integration in the THz regime with very large antenna arrays (VLAAs) is extremely complex. Thus, the wideband nature of the prospective THz data links decreases the efficiency of the generated THz beams, as we expand upon in detail later. *These two challenges, and in particular the latter challenge, provide the main motivation for this work.*

In this paper, we explore and compare the performance of different techniques for enabling directional *wideband* THz communications in the near-field. First, in Section II, we describe the results of our measurement campaign for THz communications, illustrating that extremely-high-gain antennas or, specifically, VLAAs for mobile systems, are needed for THz communications even in relatively short-range indoor deployments. In Section III, we elaborate on the near-field zone of such VLAAs and the different wavefronts that can generate beams to complement or even replace canonical beamforming in such deployments. We also explain the wideband implementation of such designs. We present our results in Section IV, where, in particular, we observe that THz Bessel beams outperform both beamforming and beamfocusing techniques in near-field scenarios. We further show a simple methodology for mitigating wideband effects with Bessel beams at THz frequencies. We conclude our paper in Section V.

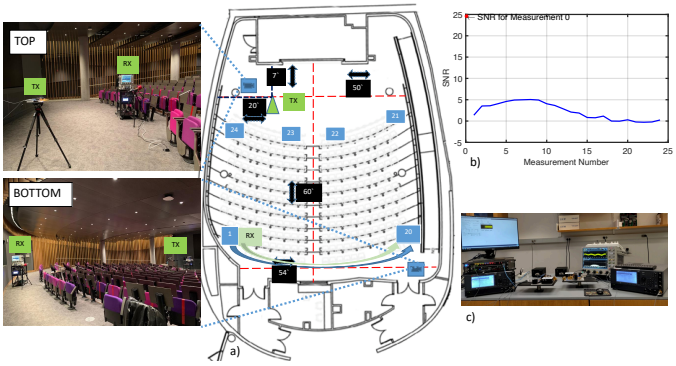

Fig. 1: A case study at 130 GHz: a) The auditorium layout, fixed Tx and RX moved to 24 spots marked within – the top and bottom insets are photos of the experiment in progress, from locations as depicted within the layout; b) SNR strength derived at respective measurement spots; and c) The TeraNova Testbed utilized for the experiment.

II. Indoor THz Links: A Measurement Campaign

A. Measurement Scenario and Hardware

To objectively demonstrate the need for VLAAs for THz communications, we conducted an experimental measurement campaign in an indoor scenario relevant to future wireless networks operating above 100 GHz. A large auditorium (275-seat capacity, as in Fig. 1(a)) in the Interdisciplinary Sciences and Engineering Complex (ISEC) at Northeastern University was selected for the measurements. A typical scenario in this setting would be, for example, where a presenter (TX) broadcasts high data feeds to the users in the audience (RX), i.e., to their tablets or XR devices [14]. In such a setting, it is extremely important to characterize the SNR at the RX in unfavorable positions. These unfavorable positions exhibit truncated signal strength from greater path loss due to longer link distances, the poor relative orientation between the TX and RX, or both.

We utilize the TeraNova testbed [15] to generate, radiate, receive, and process a 10-GHz-wide BPSK-modulated signal at 130 GHz carrier frequency. We first fix the TX location near the presenter podium, directly towards the audience. The front-end utilized a power of 0.02 W and 21 dB gain. We exploit a 38 dB gain front-end at the RX, which is placed on a pod stand with complete degrees of freedom to achieve any orientation. Twenty-four measurement spots, as marked in Fig. 1(a), are considered. Measurements 1–20 benchmark signal strength at unfavorable distances, whereas Measurements 21–24 benchmark signal strength at unfavorable orientations. Finally, Measurement 0 is specifically recorded as a reference point to highlight the SNR at a 3 m line-of-sight (LoS) configuration, where the spreading losses are reduced.

B. Key Results and Observations

The measured raw data samples are then combined and processed during the post-processing phase to produce informative performance indicators for each of the measured locations. The average SNR experienced in each of the measurement locations is illustrated in Fig. 1(b). The obtained results highlight the potential limitations in systems without VLAAs. Particularly, even in the presence of 21 dB + 38 dB $\approx$ 60 dB gain from TX and RX antennas, the resulting average SNR stays in-between 0 dB and 5 dB for all the measurements from 1 to 24. While it is theoretically possible to perform data exchange with the SNR of 5 dB, the resulting spectral efficiency will not exceed $\log_2(1 + SNR) \approx 2\,\text{bit/s/Hz}$. Hence, a 10-GHz-wide sub-THz band will feature no more than 20 Gbit/s capacity, which is very far from the desired performance indicators for THz systems [16], [17], not even accounting for the overheads of the physical and link layers.

In addition, the transmission scheme that we have considered in our campaign is BPSK; higher-order modulations require a greater threshold SNR to guarantee the same BER performance. Considering these constraints, and the aforementioned measurements, it becomes clear that the use of VLAAs in typical indoor settings is critical at frequencies above 100 GHz. The design of these VLAAs can be simplified significantly through the utilization of intelligent reflecting surfaces (IRSs), especially since the instantaneous bandwidth of VLAAs is usually on the order of $1/\tau$, where τ is the propagation delay across the array aperture [18].

III. Wideband Near-field THz Communications

A. The Superposition Principle and the Array Gain

Each element of an array radiates an EM signal. The superposition of these signals then describes the amplitude of the EM signal as generated by an array aperture. For an array in the xy plane, centered at $Z = 0$, the resultant radiation can be manipulated through the application of a set of time delays across the elements of the array, to have coherent addition at the receiver. Due to the extreme complexity of true time delay lines, the time delay δt is often approximated through a phase delay $\delta\phi = kc\delta t$, where k is the wavevector and c is the speed of EM waves. Clearly, when the phases of individual elements coherently add up towards the receiver, the beam energy is concentrated in a smaller region. The question that arises is, how do we find the required distribution of phases?

B. Wideband Considerations

Regardless of the methodology utilized to find the phases, these must then be actually applied across the array elements. For such a setup, a codebook $C(\Phi)$ is utilized. Since the codebook involves phase delays that are a function of the wavevector, we can expect:

$$C(\Phi) = f(k), \tag{1}$$

where k is the wavevector. In a wideband system, the bandwidth of the system $B = [f_{min}, f_{max}]$, centered around a design frequency f_0. Thus, the codebook is found as a function of this central design wavevector k_0:

$$C(\Phi) = f(k_0), \tag{2}$$

that is then unchanged across the range of the frequencies. The equivalent codebooks $C(\Phi)_k$ that are then effectively applied

to the other frequencies of this wideband system depend on both the wavevector k as well as the "central codebook" $C(\Phi)$:

$$C(\Phi)_k = f(k, C(\Phi)). \tag{3}$$

C. Beamforming – The Plane Wave Approximation

The simplest methodology for finding the required phase distribution for coherent addition is to assume that the receiver is infinitely away from the array. In such a setup, an array in the x-y plane radiates a plane wave specified by spherical coordinates (θ, ϕ, ρ) [19]. Then, the required phases are stored in a codebook, $C(\Phi)$, given as [7]:

$$C(\Phi) = -k_0(d\sin\theta(\Delta x\cos\phi + \Delta y\sin\phi)), \tag{4}$$

with d as the separation between the elements. Setting Δx or Δy to 1 signifies a progression in the x or y direction, respectively. From (3), we observe:

$$C(\Phi)_k = -\alpha k(d\sin\theta(\Delta x\cos\phi + \Delta y\sin\phi)), \tag{5}$$

where $\alpha = k_0/k$. α changes across the bandwidth, indicating that while the value of the phase delay remains the same across the bandwidth, its effect doesn't. The "wideband" effect serves to produce a squint, or a slight deviation, in the resultant direction of beamsteering. Notably, for broadside radiation ($\theta = 0$), the phases all equate to zero, and there is no discernable wideband effect.

The plane-wave approximation of beamforming is applicable when the receiver is in the far field of the array. However, when VLAAs are required, the length of the array can quickly cross even hundreds of wavelengths in size, or reach a few centimeters at THz frequencies. In a VLAA with a side length L, the applicable far-field distance, or the boundary of the near-field and the far-field, D_{ff}, is found as [7]:

$$D_{ff} = 2\frac{L^2}{\lambda}, \tag{6}$$

Thus, the requirement of a massive gain, due to the very high path losses at these (sub) THz frequencies, is what constitutes the very large near-field zone. A link budget shows that arrays with gains of up to 60-70 dB may be required for very high data rates [20], [21], where the applicable far-field boundary will quickly cross most limits of envisioned applications of THz communications [21].

D. Operation in the Near field

Identifying the likely region of operation as the near field, we observe that we must adapt the operation of the array, and the determination of the codebook $C(\Phi)$, through a different technique.

1) Beamfocusing: The simplest solution is to revisit the phenomenon of beamforming, and observe that the plane wave approximation is in fact a spherical equivalent in the near-field [9]. As shown in Fig. 2(b), a lens-like operation, wherein the focal point F is equal to the distance of the receiver from the array, is desired. Here, $C(\Phi)$ is of the form [7]:

$$C(\Phi) = k(\sqrt{F^2 + (x^2 + y^2)} - F), \tag{7}$$

that serves to strip off the phases acquired from the different path length r_i of each path from an element of the array to the focal point. Equivalently,

$$C(\Phi) = e^{+jk_0r_i}. \tag{8}$$

providing an exact conjugate of the individual path distance from each element to the RX, with the convergence at a specific spot. Ultimately, however, such a technique is quite susceptible to any micro/macro mobility and needs constantly updating channel state information (CSI) as the radiation is concentrated in a focal spot. For a wideband system, we derive $C(\Phi)_k$ as in (3):

$$C(\Phi)_k = e^{+jk\alpha r_i}, \tag{9}$$

where $\alpha = k_0/k$. Thus, in the case of beamfocusing, we will observe a beam-splitting effect dependent on the percentage deviation from the carrier frequency, as the equivalent compensation of path difference, αr_i, changes with the frequency.

2) Bessel Beams – A more appealing solution?: The application of phases that serve to mimic plane waves traveling inwards on a cone produces a beam, that has a non-diffracting intensity that can be illustrated through the Bessel function [22]. Such Bessel beams, wherein a beam characterized by a non-diffracting central spot along the central axis of the so-defined cone, with concentric rings around it, are set up in the near-field of the array, and propagate to a maximum distance Z_{max}, given by [23]:

$$Z_{max} = \frac{L}{2tan(\theta)}, \tag{10}$$

where L is the side length and θ is the angle of the cone. The required codebook $C(\Phi)$ is then found as:

$$C(\Phi) = k_0\sqrt{x^2 + y^2}sin(\theta), \tag{11}$$

where θ describes the angle of the realized cone. The resultant beam profile is shown in Fig. 2(e), wherein a beam characterized by a non-diffracting central spot along the central axis of the so-defined cone, with concentric rings around it, is set up. For the wideband system, we have:

$$C(\Phi)_k = k\sqrt{x^2 + y^2}(\alpha sin(\theta)), \tag{12}$$

where $\alpha = k_0/k$ as before. Thus, in the case of Bessel beams, the wideband effect changes the angle of the cone, thereby altering the propagation range of the Bessel. More importantly, we observe that as the cone angle becomes reduced, we get a longer propagation and as the cone angle sharpens, we get a reduced propagation distance.

IV. Numerical Results

In this section, we present our results that validate and elaborate on the discussions in the previous sections. We consider an array that can provide up to 70 dB of gain, which can support THz-band communications for larger link distances. A 300 GHz design frequency (λ = 1 mm, and a bandwidth of 20%, or 60 GHz is considered with a planar array. To accurately capture the broadband effect, we restrict

the mobility of the receiver along the broadside, either towards or further from the array. In the case of more complex propagation scenarios, the impact of the environment would also play a key factor in the efficiency of each wavefront.

A. Comparison of the Radiation Efficiency

Figure 3 presents the quantitative performance of the different modes of array operation, namely beamforming (Fig. 3(a)), beamfocusing (Fig. 3(b)) and Bessel beams (Fig. 3(c)), at the limits of the bandwidth. The radiation efficiency is an often neglected parameter that directly contributes to the derived SNR by capturing how efficiently the desired wavefront has been generated [21]. Due to the massive far-field distance, beamforming is crippled. The focusing point of beamfocusing is arbitrarily chosen to coincide with the maximum efficacy of Bessel beams ($13.5\,\mathrm{m}$). We observe that although both these operating regimes can sustain the maximum efficiency at this optimal point, beamfocusing has significantly less tolerance to micro-mobility; any movement near or further to the array considerably drops the radiating efficiency. In the case of Bessel beams, the efficiency is considerably maintained.

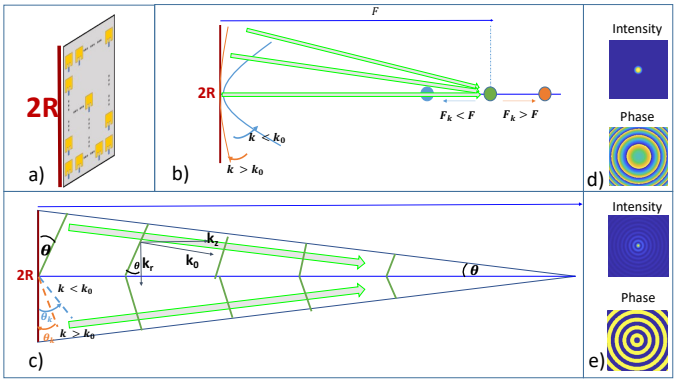

Fig. 2: a) An antenna array can be utilized to create different near-field solutions such as b) beamfocusing and c) Bessel beams. The wideband ramifications of the system affect the operation of these different wavefronts in different ways. The intensity and phase of the beamprofile in the longitudinal (cross-sectional) plane are shown in d) and e) for beamfocusing and Bessel beams, respectively.

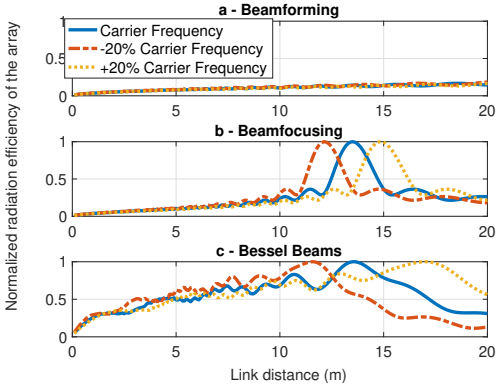

Fig. 3: Normalized radiation efficiency of a) beamforming; b) beamfocusing; c) Bessel beams.

B. Improved Wideband System Design in the Near Field

Further, we observe from Fig. 3 that across the bandwidth considered (only dependent as a percentage of the carrier frequency), beamfocusing is split into several focal spots. On the other hand, the utilization of a Bessel beam serves to provide a certain resilience to the wideband effect, since a change in the frequency only changes the cone angle, and thus the maximum distance of propagation of the resultant Bessel.

We further illustrate this effect in Fig. 4. We fix the link distance to $13.5\,\mathrm{m}$, which was the optimal focal point for a $300\,\mathrm{GHz}$ carrier. It is observed in Fig. 4(a), that when the system is designed at f_0, beamfocusing has a significant drop in efficiency across the bandwidth. Bessel beams are resilient with a reduced drop. The drop is more pronounced for the portion of the bandwidth that is below the design frequency, as the range of the Bessel is decreased in those instances. Although beamforming does not face any losses due to the fact that the phase is set as zero, the absolute value of the efficiency is too low to be considered an apt design.

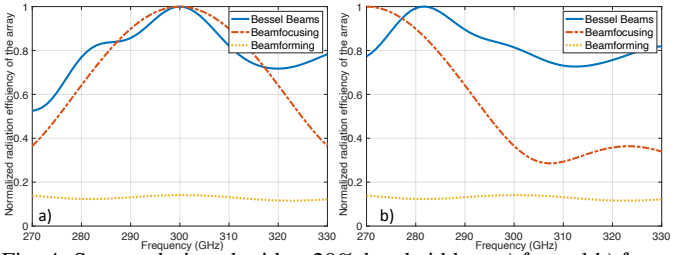

Fig. 4: System designed with a 20% bandwidth at a)f_0; and b)f_{min}.

Hence, we observe that the use of Bessel beams and a simple sanity check helps counter the wideband effects significantly – when the system is designed for the *lowest frequency comprising the system bandwidth*, nearly the same performance can be expected across the entire bandwidth, as in Fig. 4(b). This is an important practical insight, exclusive to Bessel beams: designing the system with the lowest frequency in mind allows concentrating most of the energy near the target receiver. The observed effect is another advantage of using Bessel beams for THz communications in the near field.

V. Conclusions

The very high path losses at (sub) THz frequencies make the near-field region a likely scenario for future wireless communication scenarios. The manifestations of near-field, wideband, and mobile system implementation make canonical beamforming and beamfocusing unattractive solutions. Bessel beams, designed at the lower end of the wideband system, can significantly mitigate the problems of accurately providing the improved radiation gain that is necessary for sustaining reliable, ultra-high data rate links at such frequencies.

References

[1] I. F. Akyildiz, J. M. Jornet, and C. Han, "Terahertz band: Next frontier for wireless communications," *Physical Communication*, vol. 12, pp. 16–32, 2014.

[2] T. S. Rappaport, Y. Xing, O. Kanhere, S. Ju, A. Madanayake, S. Mandal, A. Alkhateeb, and G. C. Trichopoulos, "Wireless communications and applications above 100 GHz: Opportunities and challenges for 6G and beyond," *IEEE Access*, vol. 7, pp. 78 729–78 757, 2019.

[3] J. M. Jornet and I. F. Akyildiz, "Channel modeling and capacity analysis for electromagnetic wireless nanonetworks in the terahertz band," *IEEE Transactions on Wireless Communications*, vol. 10, no. 10, pp. 3211–3221, 2011.

[4] P. Boronin, V. Petrov, D. Moltchanov, Y. Koucheryavy, and J. M. Jornet, "Capacity and throughput analysis of nanoscale machine communication through transparency windows in the terahertz band," *Nano Communication Networks*, vol. 5, no. 3, pp. 72–82, 2014.

[5] I. F. Akyildiz, A. Kak, and S. Nie, "6G and beyond: The future of wireless communications systems," *IEEE Access*, vol. 8, pp. 133 995–134 030, 2020.

[6] I. F. Akyildiz and J. M. Jornet, "Realizing ultra-massive MIMO (1024×1024) communication in the (0.06–10) terahertz band," *Nano Communication Networks*, vol. 8, pp. 46–54, 2016, U.S. Patent No. 9,825,712, November 21, 2017 (Priority Date: Dec. 6, 2013).

[7] C. A. Balanis, *Antenna theory: analysis and design*. John Wiley & Sons, 2016.

[8] C. Liaskos, S. Nie, A. Tsioliaridou, A. Pitsillides, S. Ioannidis, and I. Akyildiz, "A novel communication paradigm for high capacity and security via programmable indoor wireless environments in next generation wireless systems," *Ad Hoc Networks*, vol. 87, pp. 1–16, 2019.

[9] K. Dovelos, S. D. Assimonis, H. Q. Ngo, B. Bellalta, and M. Matthaiou, "Electromagnetic modeling of holographic intelligent reflecting surfaces at terahertz bands," in *2021 55th Asilomar Conference on Signals, Systems, and Computers*. IEEE, 2021, pp. 415–420.

[10] J. Tan and L. Dai, "Delay-phase precoding for thz massive mimo with beam split," in *2019 IEEE Global Communications Conference (GLOBECOM)*. IEEE, 2019, pp. 1–6.

[11] S. Kalia, S. A. Patnaik, B. Sadhu, M. Sturm, M. Elbadry, and R. Harjani, "Multi-beam spatio-spectral beamforming receiver for wideband phased arrays," *IEEE Transactions on Circuits and Systems I: Regular Papers*, vol. 60, no. 8, pp. 2018–2029, 2013.

[12] S. V. Hum and J. Perruisseau-Carrier, "Reconfigurable reflectarrays and array lenses for dynamic antenna beam control: A review," *IEEE Transactions on Antennas and Propagation*, vol. 62, no. 1, pp. 183–198, 2013.

[13] I. Frigyes and A. Seeds, "Optically generated true-time delay in phased-array antennas," *IEEE Transactions on Microwave Theory and Techniques*, vol. 43, no. 9, pp. 2378–2386, 1995.

[14] V. Petrov, M. Gapeyenko, S. Paris, A. Marcano, and K. I. Pedersen, "Standardization of Extended Reality (XR) over 5G and 5G-Advanced 3GPP New Radio," 2022.

[15] P. Sen, V. Ariyarathna, A. Madanayake, and J. M. Jornet, "Experimental wireless testbed for ultrabroadband terahertz networks," in *Proceedings of the 14th International Workshop on Wireless Network Testbeds, Experimental evaluation & Characterization*, 2020, pp. 48–55.

[16] ATISn, "NextG Alliance," 2021, accessed: December 10, 2019.

[17] W. Jiang, B. Han, M. A. Habibi, and H. D. Schotten, "The road towards 6g: A comprehensive survey," *IEEE Open Journal of the Communications Society*, vol. 2, pp. 334–366, 2021.

[18] X. Ye, D. Zhu, Y. Zhang, S. Li, and S. Pan, "Analysis of photonics-based rf beamforming with large instantaneous bandwidth," *Journal of Lightwave Technology*, vol. 35, no. 23, pp. 5010–5019, 2017.

[19] D. Headland, Y. Monnai, D. Abbott, C. Fumeaux, and W. Withayachumnankul, "Tutorial: Terahertz beamforming, from concepts to realizations," *APL Photonics*, vol. 3, no. 5, p. 051101, 2018.

[20] C. Lin and G. Y. Li, "Indoor terahertz communications: How many antenna arrays are needed?" *IEEE Transactions on Wireless Communications*, vol. 14, no. 6, pp. 3097–3107, 2015.

[21] A. Singh, A. J. Alqaraghuli, and J. M. Jornet, "Wavefront engineering at terahertz frequencies through intelligent reflecting surfaces," in *2022 IEEE 23rd International Workshop on Signal Processing Advances in Wireless Communication (SPAWC)*. IEEE, 2022, pp. 1–5.

[22] J. Durnin, "Exact solutions for nondiffracting beams. I. the scalar theory," *JOSA A*, vol. 4, no. 4, pp. 651–654, 1987.

[23] J. Durnin, J. Miceli, and J. H. Eberly, "Comparison of bessel and gaussian beams," *Optics letters*, vol. 13, no. 2, pp. 79–80, 1988.